Pointwise Nonlinear Scaling for Reaction-Diffusion-Equations

Martin Weiser

February 26, 2009

This is the revised version that will appear in *Applied Numerical Mathematics* (DOI 10.1016/j.apnum.2009.01.010).

Abstract

Parabolic reaction-diffusion systems may develop sharp moving reaction fronts which pose a challenge even for adaptive finite element methods. We propose a method to transform the equation into an equivalent form that usually exhibits solutions which are easier to discretize, giving higher accuracy for a given number of degrees of freedom. The transformation is realized as an efficiently computable pointwise nonlinear scaling that is optimized for prototypical planar travelling wave solutions of the underlying reaction-diffusion equation. The gain in either performance or accuracy is demonstrated on different numerical examples.
AMS MSC 2000: 65M60, 65M50

Keywords: reaction-diffusion equations, travelling waves, nonlinear scaling, discretization error

1 Introduction

Reaction-diffusion equations are used to model a tremendous amount of effects, in particular in chemistry, biology, or material sciences. They describe the spatio-temporal distribution of one or more species subject to diffusion and nonlinear interaction. Due to their importance in practical applications, a considerable amount of effort has been spent on the numerical solution [9].

One of the outstanding properties of reaction-diffusion equations is the existence of travelling waves, which are moving reaction fronts. An accurate representation of reaction fronts is usually necessary in computations to capture the front speed correctly. If the diffusion is small compared to the computational domain and the

reaction speed, the reaction fronts can be rather sharp. A quantitatively faithful resolution of sharp reaction fronts is quite challenging for numerical methods, since a rather small mesh size is required. Uniform meshes are often inefficient or even useless due to the exceedingly large number of unknowns they incur. For this reason, adaptive mesh refinement techniques are widely used, in particular for finite element discretizations [12].

In Rothe's method, standard h-, p-, and hp-refinement are used for the stationary elliptic problems arising in each time step, along with mesh coarsening in regions of the domain which the front has left behind. More specialized approaches such as anisotropic refinement [1,11] or different refinement levels for variables with different smoothness [18] are effective, but difficult to implement, in particular in combination with maintaining a mesh hierarchy for geometric multigrid solvers. Domain transformations and vertex relocations, so-called r-refinement, have been proven to be efficient for one-dimensional problems [10, 16] and have also been studied for 2D and 3D problems with some success [2, 13]. Drawbacks are the overhead of additional PDEs describing the mesh movement and the difficult treatment of geometrically complex boundaries.

Unlike the linear wave equation that advances waves of arbitrary shape with the same speed, reaction-diffusion equations often allow only a small number of wave shapes to be propagated at all, with the wave speed depending on the wave shape. Thus, the local solution structure is to some extent determined by the travelling wave solutions of the reaction-diffusion equation. In this paper, we try to exploit this fact and propose an analytical preprocessing based on planar travelling waves. The preprocessing is a pointwise nonlinear scaling of the range that aims at smoothing out sharp reaction fronts. The approach requires analytical preprocessing and is therefore much less general than mesh refinement, but since only a pointwise scaling is involved, the implementation effort is negligible and the computational overhead rather small.

The remainder of the paper is organized as follows. In section 2, the concept of pointwise nonlinear scaling is introduced formally. The main section 3 is devoted to the development of a framework for computing optimal scalings for spatial finite element discretizations. This is transferred to time discretizations in the following section 4. Finally, scaling for spatio-temporally adaptive methods is considered in section 5.

2 Pointwise Nonlinear Scaling

Let us consider a simple scalar reaction-diffusion equation of the form

$$\begin{aligned} &\partial_t u = \nabla \cdot (\kappa \nabla u) + f(u) && \text{in } \Omega \\ &u = u_D && \text{on } \partial\Omega_D \\ &\kappa \partial_n u = \gamma(u_N - u) && \text{on } \partial\Omega_N = \partial\Omega \backslash \partial\Omega_D. \end{aligned} \tag{1}$$

Here, Ω is a domain in $\mathbb{R}^d$ and $f : \mathbb{R} \to \mathbb{R}$ is a smooth function.

We introduce a smooth, strictly monotone increasing function $\zeta : \mathbb{R} \to \mathbb{R}$ and its inverse $\vartheta = \zeta^{-1}$ as pointwise nonlinear scalings of the range of u. Now the scaled variable $u_\zeta = \zeta(u)$ satisfies the reaction-diffusion equation

$$\begin{aligned} &\vartheta'(u_\zeta)\partial_t u_\zeta = \nabla \cdot (\kappa \vartheta'(u_\zeta) \nabla u_\zeta) + f(\vartheta(u_\zeta)) && \text{in } \Omega \\ &u_\zeta = \zeta(u_D) && \text{on } \partial\Omega_D \\ &\vartheta'(u_\zeta)\kappa \partial_n u_\zeta = \gamma(u_N - \vartheta(u_\zeta)) && \text{on } \partial\Omega_N = \partial\Omega \backslash \partial\Omega_D \end{aligned} \tag{2}$$

for all t, such that the following diagram commutes:

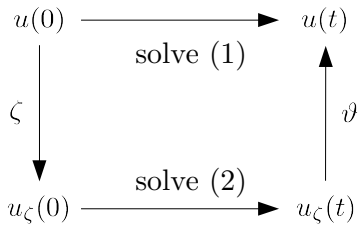

In this sense, the exact solution is invariant under pointwise nonlinear scaling.

If in actual computation the solution step is substituted by some discretization, e.g., finite elements combined with implicit Runge-Kutta methods, the commutativity of the diagram is lost. Since it is impossible to devise a discretization that is invariant under arbitrary smooth nonlinear scalings, we are left with the task of explicitly choosing a scaling ζ. A natural choice would be the one minimizing the discretization error for a given discretization, or, essentially equivalent, minimizing the computational complexity for obtaining a desired accuracy. On that score, the identity (id) is usually not the scaling of choice, even though it leads to the particularly simple formulation (1) of the more general problem (2).

Note that finding an optimal scaling for a given problem is at least as difficult as solving the original problem. In the following we will therefore characterize quasi-optimal scalings in terms of planar travelling wave solutions, in the hope that the accuracy gain transfers to more general problems with a richer solution structure.

3 Scaling for Spatial Discretization

To begin with, we address the spatial discretization, since this is usually the most costly aspect in discretizing reaction-diffusion equations. First we need to construct a quantitative characterization of optimal scalings. A reasonable choice is to minimize the product $E_x(\zeta)W_x(\zeta)$ of the spatial discretization error $E_x(\zeta)$ and the computational complexity $W_x(\zeta)$. Additionally we have the conflicting goal of aiming at smooth scalings that do not introduce discontinuities or very large values of higher derivatives of the scaled solution u_ζ. We thus introduce a regularization parameter $\alpha > 0$ and define the desired scaling as a minimizer of

$$\min_{\zeta} \; E_x(\zeta)W_x(\zeta) + \frac{\alpha}{2}\|\zeta^{(s)}\|^2_{L^2(\mathbb{R})} \quad \text{s.t. } \zeta' > 0, \tag{3}$$

where $s > 1$ is chosen appropriately for the underlying discretization of u_ζ. For finite elements of order p, a value of $s = p + 1$ seems reasonable.

Discretization error model. Using finite elements of order p on a triangulation $\mathcal{T}$ of the domain Ω for discretizing the scaled solution u_ζ as u^h_ζ, we assume the following local approximation error estimate holds on each element $T \in \mathcal{T}$ of the mesh:

$$\|u_\zeta - u^h_\zeta\|_{L^2(T)} \leq c h_T^{p+1} |u_\zeta|_{H^{p+1}(T)}$$

Here, c is some generic constant independent of the diameter h_T of the element T. The estimate holds if $u_\zeta \in H^{p+1}(\Omega)$.

Defining the discretized unscaled solution as $u^h = \vartheta(u^h_\zeta)$, we obtain the following asymptotic error estimates for the unscaled solution:

$$\begin{aligned}
\|u - u^h\|_{L^2(T)} &= \|\vartheta(u_\zeta) - \vartheta(u^h_\zeta)\|_{L^2(T)} \\
&\leq \|\vartheta'(u_\zeta)\|_{L^\infty(T)} \|u_\zeta - u^h_\zeta\|_{L^2(T)} + \mathcal{O}(\|u_\zeta - u^h_\zeta\|^2_{L^2(T)}) \\
&\leq c h_T^{p+1} \|\vartheta'(u_\zeta)\|_{L^\infty(T)} |u_\zeta|_{H^{p+1}(T)} + \mathcal{O}(\|u_\zeta - u^h_\zeta\|^2_{L^2(T)})
\end{aligned} \tag{4}$$

As a continuous model of (4) we introduce the local mesh size $h : \Omega \to \mathbb{R}_+$ and define the local L^2 error density pointwise as

$$e_{x\zeta}(x) = h(x)^{p+1} \vartheta'(u_\zeta(x)) |u^{(p+1)}_\zeta(x)|, \tag{5}$$

such that we can estimate the overall error by

$$\|u - u^h\|_{L^2(\Omega)} \lessapprox c \|e_{x\zeta}\|_{L^2(\Omega)}.$$

Consequently, we define our error quantity as

$$E_x(\zeta) = \|e_{x\zeta}\|^2_{L^2(\Omega)}.$$

In passing we note that a slightly longer computation yields a related error model

$$\bar{e}_{x\zeta}(x) = h(x)^{p+1} \left(\vartheta'(u_\zeta(x)) + \vartheta''(u_\zeta(x))|\nabla u_\zeta(x)|\right) |u_\zeta^{(p+1)}(x)|$$

for the H^1 error, such that $\|u - u^h\|_{H^1(\Omega)} \lessapprox c\|\bar{e}_{x\zeta}\|_{L^2(\Omega)}$. For notational simplicity, however, we will concentrate on the L^2 estimates.

Complexity model. Using an efficient solver, the computational complexity for computing u_ζ^h is proportional to the number of elements in the mesh. From the mesh size distribution h we can approximate the number of elements as

$$W_x(\zeta) = \int_\Omega h(x)^{-d}\, dx \tag{6}$$

for isotropic elements.

Mesh models. Note that both E_x and W_x and hence the minimizer ζ of (3) do depend on the mesh size distribution h. Here we restrict our attention to meshes resulting from the two commonly encountered mesh refinement strategies: uniform meshes and adaptively refined meshes.

For uniformly refined meshes we may assume h to be constant in (5), such that

$$E_x(\zeta)W_x(\zeta) = c\,\|\vartheta'(u_\zeta)u_\zeta^{(p+1)}\|^2_{L^2(\Omega)}. \tag{7}$$

For adaptively refined meshes we assume equilibration of local errors (4), which in our continuous model means that $e_{x\zeta}$ is constant. We then have

$$h(x) = c\left|\vartheta'(u_\zeta(x))u_\zeta^{(p+1)}(x)\right|^{-1/(p+1)},$$

such that

$$E_x(\zeta)W_x(\zeta) = c\int_\Omega \left|\vartheta'(u_\zeta)u_\zeta^{(p+1)}\right|^{d/(p+1)}\, dx \tag{8}$$

holds.

Solution model. Unfortunately, the unknown solution u enters into $e_{x\zeta}$ via u_ζ. Thus we need to find an easily computable substitute that exhibits the same local structure and features as the solution u.

We assume that in most of the domain Ω the solution looks locally like a planar travelling wave. This assumption neglects effects frequently encountered in reaction-diffusion patterns, such as curvature-dependent wave speed, anisotropic diffusion, a continuum of wave forms and speeds, and boundary effects. Nevertheless, the planar travelling wave assumption should capture the bulk of the local solution

structure mostly correct and is moreover analytically and numerically tractable due to its inherent one-dimensional nature. Thus, we look for nonlinear scalings that are optimal for planar travelling waves.

Let us assume that for some velocity direction $v \in \mathbb{R}^d$ with $|v| = 1$ and some wave speed $\sigma \geq 0$, (1) has a sufficiently smooth planar travelling wave solution $u(x,t) = w(-v^T x + \sigma t)$ on $\mathbb{R}^d$, with $w : \mathbb{R} \to [0,1]$ being essentially constant outside some interval $[a,b]$. Now we can substitute w for u and $[a,b]$ for Ω.

Practical restrictions. For the numerical computation of ζ to be practical, one more aspect has to be considered. Since the range of w is assumed to be contained in $[0,1]$, we may essentially restrict our attention to scalings mapping $[0,1]$ into itself. However, actual solutions may well exceed this range, such that ζ needs to be represented on whole $\mathbb{R}$. Since the travelling wave substitute w does not provide any information outside $[0,1]$, we select the most simple representation: linear extension. We therefore restrict ζ to the admissible set

$$Z = \{\zeta : \mathbb{R} \to \mathbb{R} | \zeta(0) = 0, \zeta(1) = 1, \zeta' > 0, \operatorname{supp} \zeta^{(k)} \subset [0,1] \text{ for } k = 2, \dots, s\}.$$

Combining all above considerations, we end up with the optimization problems

$$\min_{\zeta \in Z} \int_a^b \left| \vartheta'(w_\zeta) w_\zeta^{(p+1)} \right|^r \, dx + \frac{\alpha}{2} \|\zeta^{(s)}\|^2_{L^2([0,1])} \tag{9}$$

to solve for optimal scalings ζ for uniformly ($r = 2$) and adaptively ($r = d/(p+1)$) refined meshes, respectively.

One particularly nice property of this approach to select optimal scalings is that the result is essentially independent of the diffusion coefficient κ determining the width of the reaction front.

Lemma 3.1. *Let $u(x,t) = w(x + \sigma t)$ be a travelling wave solution of (1) for $\kappa = 1$ on $\Omega = \mathbb{R}$ and $\zeta(\alpha) = \arg\min_\xi \left(E_x(\xi) W_x(\xi) + \frac{\alpha}{2} \|\xi^{(s)}\|^2_{L^2(\Omega)} \right)$ the associated optimal scaling. Then, for every $0 < \kappa \in \mathbb{R}$, $\zeta_\kappa(\alpha) = \zeta(\kappa^{1/2 - r(p+1)/2} \alpha)$ is an optimal scaling associated to the travelling wave solution $u_\kappa(x,t) = w(x/\sqrt{\kappa} + \sigma t)$ of (1) on $\Omega = \mathbb{R}$.*

Proof. A short calculation shows that $u_\kappa(x,t) = w(x/\sqrt{\kappa} + \sigma t)$ is indeed a travelling wave solution of (1). Without loss of generality we assume $t = 0$. By the chain rule, we have

$$\partial_x^{p+1} \zeta(u_\kappa(x)) = \partial_x^{p+1} \zeta(w(x/\sqrt{\kappa})) = \kappa^{-(p+1)/2} \partial_\xi^{p+1} \zeta(w(\xi))$$

for $\xi = x/\sqrt{\kappa}$. We introduce the notation E_x^κ and W_x^κ to make the dependence of E_x and W_x on κ explicit. By the substitution rule, we have

$$\begin{aligned}
E_x^\kappa(\zeta) W_x^\kappa(\zeta) &= \int_{\mathbb{R}} \left| \vartheta'(u_{\kappa\zeta}(x)) u_{\kappa\zeta}^{(p+1)}(x) \right|^r \, dx \\
&= \int_{\mathbb{R}} \left| \zeta'(w(x/\sqrt{\kappa}))^{-1} \partial_x^{p+1} \zeta(w(x/\sqrt{\kappa}) \right|^r \, dx \\
&= \int_{\mathbb{R}} \left| \zeta'(w(\xi))^{-1} \kappa^{-(p+1)/2} \partial_\xi^{p+1} \zeta(w(\xi)) \right|^r \sqrt{\kappa} \, d\xi \\
&= \kappa^{1/2 - r(p+1)/2} \int_R \left| \zeta'(w(\xi))^{-1} \partial_\xi^{p+1} \zeta(w(\xi)) \right|^r \, d\xi \\
&= \kappa^{1/2 - r(p+1)/2} E_x^1(\zeta) W_x^1(\zeta).
\end{aligned}$$

Choosing $\alpha_\kappa = \kappa^{1/2 - r(p+1)/2} \alpha$ results in a simple scaling of the objective in (9) that does not change the minimizers. □

3.1 Numerical Examples

In the previous section, we have characterized optimal scalings as minimizers of the work per accuracy ratio. The associated objective yields a prediction of the error reduction for uniform meshes or the savings in computational work for adaptive meshes. However, this prediction comes from an idealized model situation. The error and work model are continuous and do not take the necessarily discrete structure of the mesh into account. Moreover, the error model is just a worst-case model with limited predictive power for an actual situation.

The most important simplification is that, the characterization of ζ is based on planar travelling waves. In 2D/3D problems, the solution structure can be much richer due to source terms, boundary conditions, and complex geometries. It is not clear a priori, to which amount the error reduction transfers to more complex settings. The first numerical example given in Section 3.1.1 is therefore a simple 1D interpolation problem suitable for testing the work and error models.

3.1.1 1D Travelling Wave Approximation

As a first illustration of the effect of pointwise nonlinear scaling on the discretization error we consider the piecewise linear interpolation of a reaction front. As an arbitrary front shape we select the hyperbolic tangent on the interval $\Omega_1 = [-5, 5]$:

$$w(x) = \frac{1}{2}(\tanh x + 1)$$

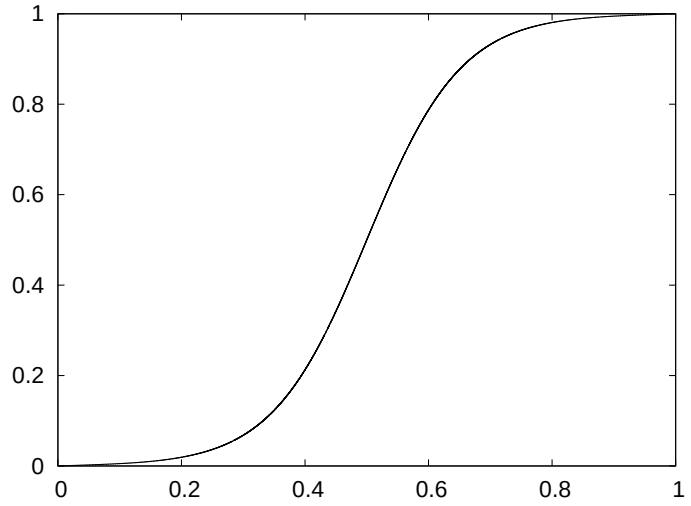

Figure 1: Nonlinear scaling ζ^{-1} for equidistant interpolation of the hyperbolic tangent.

Equidistant Interpolation. First, we approximate ζ by solving (9) with $r = 2$ numerically using lpopt [19] on a simple equidistant finite difference discretization. Since here we only aim at approximating w, we choose a rather small regularization parameter $\alpha = 10^{-12}$. The resulting scaling is shown in Fig. 1. That the shape of ζ^{-1} is very close to the hyperbolic tangent itself is to be expected: This way, with a relatively large linear interpolation segment, the curved shape of the hyperbolic tangent can be approximated very well.

The obtained values for the estimated interpolation error are $\|e_x\|_{L^2(\Omega)} = 0.5164$ for the original and $\|e_{x\zeta}\|_{L^2(\Omega)} = 0.0090$ for the scaled problem, the ratio of which gives an estimated error reduction factor of 57.2. The same ratio is obtained using the H^1 norm for measuring errors. Then, both w and w_ζ are piecewisely linearly interpolated on an equidistant grid of $2^n + 1$ points, resulting in $I^n w$ and $I^n w_\zeta$, respectively. The errors $\varepsilon_x^n = w - I^n w$ and $\varepsilon_{x\zeta} = w - \vartheta(I^n w_\zeta)$ are evaluated on a further refined grid. The results given in Table 1 coincide very well with the prediction. The slight deterioration in the error reduction factor, which is visible for $n = 11$ in particular for the H^1-error, can be attributed to the approximate representation of ζ.

Adaptive Interpolation. As a second experiment, we solve (9) with $r = d/(p+1)$, again choosing $\alpha = 10^{-12}$. The resulting scaling is very close to its counterpart for equidistant interpolation, in fact, the difference is imperceptible on the scale of Fig. 1. The quotient of the obtained values for $\int h(x)^{-d} dx$ of 2.37 and 0.247 for the original and scaled problem, respectively, predicts a reduction in the number of interpolation nodes by a factor of 9.6. Then w and w_ζ are interpolated adaptively

n	$\|\varepsilon_x\|_{L_2}$	$\|\varepsilon_{x\zeta}\|_{L_2}$	ratio	$\|\varepsilon_x\|_{H^1}$	$\|\varepsilon_{x\zeta}\|_{H^1}$	ratio
0	6.447e-1	1.542e-1	4.181	4.831e-1	1.775e-1	2.722
1	6.447e-1	1.542e-1	4.181	4.831e-1	1.775e-1	2.722
2	2.887e-1	4.155e-3	69.500	3.723e-1	6.141e-3	60.625
3	7.692e-2	1.425e-3	53.981	1.944e-1	3.744e-3	51.919
4	1.801e-2	3.354e-4	53.697	9.161e-2	1.704e-3	53.777
5	4.576e-3	7.985e-5	57.305	4.637e-2	8.099e-4	57.255
6	1.149e-3	2.009e-5	57.201	2.327e-2	4.068e-4	57.185
7	2.876e-4	5.028e-6	57.204	1.164e-2	2.036e-4	57.196
8	7.192e-5	1.257e-6	57.205	5.822e-3	1.018e-4	57.183
9	1.798e-5	3.144e-7	57.202	2.910e-3	5.095e-5	57.118
10	4.496e-6	7.864e-8	57.166	1.453e-3	2.556e-5	56.837
11	1.124e-6	1.968e-8	57.099	7.222e-4	1.292e-5	55.911

Table 1: Approximation errors for piecewise linear interpolation I_n of hyperbolic tangent on the interval [-5,5]. n is the number of uniform refinements.

TOL	n	n_ζ	ratio	m_ζ
10^{-2}	14	5	2.8	5
10^{-3}	38	8	4.8	8
10^{-4}	115	15	7.7	17
10^{-5}	375	38	9.9	46
10^{-6}	1130	114	9.9	144
10^{-7}	3579	372	9.6	435

Table 2: Number of nodes for adaptive interpolation of tanh.

by bisecting the subinterval with the largest L^2 error contribution until a given tolerance for the overall L^2-error estimate is reached. The number of interpolation nodes is reported in Table 2 as n for interpolating w, n_ζ for interpolating w_ζ, and m_ζ for interpolating w_ζ with the scaling ζ obtained for the uniform setting above.

We conclude that the continuous worst-case model for the work per accuracy ratio performs fairly well, and that, despite the minor difference in the scalings, considering different model variants for uniform and adaptive refinement is justified by the small, but clearly visible difference of the results.

3.1.2 Scalar Reaction-Diffusion Equation

The effect of solution structures differing from planar travelling waves on the effectivity of the proposed nonlinear scaling are studied at the simple scalar reaction-diffusion equation

$$\partial_t u = \kappa \Delta u + u(1-u)(u-a). \tag{10}$$

Planar travelling wave solutions $u(x,t) = w(-v^T x + \sigma t)$ with $|v| = 1$ moving in direction v with speed $\sigma = \sqrt{\kappa}\frac{1-2a}{\sqrt{2}}$ are known analytically:

$$w(z) = \left(1 + \exp\left(-\frac{z}{\sqrt{2\kappa}}\right)\right)^{-1}.$$

We employ the method of lines and first discretize the space using linear finite elements on uniform red refinements of Ω for different refinement levels n, translating (10) into an ODE. The implementation is done on top of DUNE [4, 5].

A scaling ζ is computed for minimizing the L^2-error by approximately solving (9) for $r = 2$. Since the following test cases are not perfect planar travelling waves, a more conservative regularization parameter $\alpha = 10^{-8}$ is used for linear finite elements ($p = 1$), giving a predicted error reduction factor $E_x(\mathrm{id})/E_x(\zeta) \approx 22$. Quadratic elements ($p = 2$) seem to react more sensitively to deviations from the travelling wave shape, such that we use $\alpha = 10^{-6}$ with a predicted error reduction factor of 13.

As an example that is not exactly a planar wave we consider the coalescence of circular reaction fronts. These fronts are curved and therefore deviate from the planar travelling wave shape. At the tip of the groove that occurs just after fronts touch, the curvature of the joint front is particularly high, such that pronounced deviations from the planar travelling wave shape are to be expected. We start at $t = 0$ with circular fronts centered at the points of $(2\mathbb{Z})^2$ in $\Omega = \mathbb{R}^2$ and exploit periodicity and symmetry to restrict the computation to the triangle $\bar{\Omega} = \{x \in [0,1]^2 : x_1 \geq x_2\}$ with homogeneous Neumann boundaries. We choose $\kappa = 0.0009$, $a = 0$, and $u(x,0) = w(\frac{1}{3} - |x|)$. Time stepping is performed using a linearly implicit Euler scheme extrapolated to order 4 (cf. [7]). Focusing on the spatial discretization effect, the fixed time step size $\tau = 1/8$ is chosen such that the spatial discretization error dominates. The final time is $T = 30$, just after the wave fronts have merged (see Fig. 2 left). Note that at the front vertex where the reaction fronts touch the solution structure is distinctly different from the travelling wave solution, whereas before it locally looks rather similar to a planar travelling wave.

On each refinement level n, the spatial errors at $t = T/2$ and $t = T$, $\varepsilon_x^n = u^n - u$ and $\varepsilon_{x\zeta}^n = \vartheta(u_\zeta^n) - u$, respectively, have been approximated using $\vartheta(u_\zeta^N)$ instead of u. In fact, u_ζ^N is the most accurate solution obtained. For $n = 4$, the errors at $t = T$ are shown in Fig. 2 (right). Note that the error ε_x^4 of the unscaled solution is mainly caused by an offset in the front position, that is accumulated during the propagation. With relatively large elements, the front speed of the FE solution is too large. The error $\varepsilon_{x\zeta}^4$ of the scaled solution is significantly smaller. Moreover, the dominating error contribution stems in fact from the region where the solution shape differs from the travelling wave shape. In contrast to the unscaled result, a structural error contribution due to a wrong front position is not visible.

Error norms and their ratios are given in Table 3. It is apparent that as long as the solution structure is indeed similar to the planar travelling wave ($t = 15$),

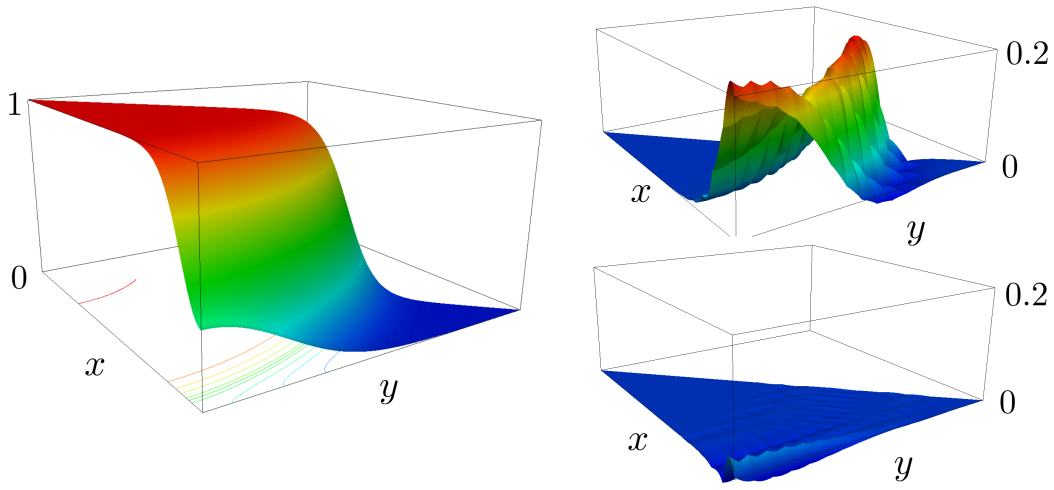

Figure 2: Left: Merging reaction fronts of (10) at final time $t = T$. Right: errors of the unscaled (top) and scaled (bottom) linear FE solution. Note that the error of the scaled solution is scaled back and hence directly comparable to the unscaled error.

		linear FE ($N = 9$)			quadratic FE ($N = 8$)		
t	n	$\|\varepsilon_x\|_{L_2}$	$\|\varepsilon_{x\zeta}\|_{L_2}$	ratio	$\|\varepsilon_x\|_{L_2}$	$\|\varepsilon_{x\zeta}\|_{L_2}$	ratio
15	1				1.82e-1	2.26e-2	8.1
	2	1.83e-1	9.67e-3	18.9	4.22e-2	8.17e-3	5.2
	3	7.71e-2	3.25e-3	23.7	8.55e-3	6.20e-4	13.8
	4	2.48e-2	6.51e-4	38.1	8.41e-4	5.01e-5	16.8
	5	6.62e-3	1.51e-4	43.8	8.34e-5	5.45e-6	15.3
	6	1.68e-3	3.67e-5	45.8	9.24e-6	6.73e-7	13.7
	7	4.21e-4	8.78e-6	47.9			
30	1				3.25e-1	3.29e-2	9.9
	2	3.29e-1	1.82e-2	18.0	1.12e-1	1.48e-2	7.5
	3	1.75e-1	5.44e-3	32.2	1.75e-2	2.25e-3	7.8
	4	5.48e-2	1.98e-3	27.7	1.58e-3	2.49e-4	6.4
	5	1.41e-2	5.03e-4	28.1	1.32e-4	2.85e-5	4.6
	6	3.54e-3	1.26e-4	28.1	1.25e-5	3.59e-6	3.5
	7	8.85e-4	3.08e-5	28.8			

Table 3: Spatial discretization error for the scalar reaction-diffusion equation (10).

the expectations are well met, with results even better than predicted for linear elements. As soon as the solution structure changes significantly, the accuracy improvement is less pronounced and drops below the value predicted for the ideal situation, in particular for quadratic finite elements. However, the dominant error of the scaled solution is confined to the small region in space and time where the reaction fronts merge. Further error reduction by adaptive mesh refinement would be less costly than in the unscaled case, where the dominant error is distributed along the whole reaction front.

As a final remark we note that boundary conditions of Dirichlet or Robin type can be expected to have a similar effect on the accuracy gain as the merging of reaction fronts in this example. The influence of homogeneous Neumann conditions depends on the relative angle between the wave front and the boundary.

4 Scaling for Time Discretization

Up to now, only the spatial discretization error has been considered. However, a nonlinear scaling ζ may also affect the integration error of time stepping schemes. In particular, the time step is essentially limited by the ratio of width and speed of the reaction front. While the front speed is invariant under nonlinear scaling, the front width is not, which should give the opportunity to design scalings that allow to take large time steps.

4.1 Optimal Scaling

The error of usual implicit single-step time stepping schemes Φ^τ approximating the evolution Φ with convergence order q is asymptotically bounded in terms of the $q+1$-th derivative of the solution as

$$|u(t+\tau) - \Phi^\tau(u(t))| \leq c \left|\partial_t^{q+1} u(t)\right| \tau^{q+1} + \mathcal{O}(\tau^{q+2}) \tag{11}$$

with some generic constant c independent of the time step size τ. We assume that (11) holds locally almost everywhere in Ω. Again, scaling back the propagation error of the scaled solution u_ζ to the original setting, the error of a single time step is asymptotically bounded by

$$|\vartheta(u_\zeta(t+\tau)) - \vartheta(\Phi^\tau(u_\zeta(t)))| \leq c\vartheta'(u_\zeta(t)) \left|\partial_t^{q+1} u_\zeta(t)\right| \tau^{q+1} + \mathcal{O}(\tau^{q+2}).$$

Note that errors need not be damped out in nonlinear parabolic equations. In particular, errors in the front position will be propagated forever. Thus we presume the local integration errors sum up. Again substituting u_ζ by a travelling wave w_ζ, we define the global propagation error density at time t

$$e_{t\zeta} = \vartheta'(u_\zeta(t))\partial_t^{q+1} u_\zeta(t)\tau^q = \vartheta'(w_\zeta)\partial_t^{q+1} w_\zeta(-v^T \cdot + \sigma t)\tau^q = \vartheta'(w_\zeta)\sigma^{q+1} w_\zeta^{(q+1)}\tau^q. \tag{12}$$

Since u_ζ is a travelling wave, we may restrict our attention to $t = 0$ and constant step sizes. The amount of work for a fixed time interval is then $W_t = \tau^{-1}$. We therefore have to minimize the quantity

$$\tau^{q-1}\sigma^{q+1}\|\vartheta'(w_\zeta)w_\zeta^{(q+1)}\|^2_{L^2(\Omega_1)}.$$

The time step enters only as a constant multiplicative factor and has no impact on the minimizer if the regularization parameter α is scaled appropriately, such that we may discard τ and arrive at the minimization problem

$$\min_{\zeta\in Z} \int_a^b \left|\vartheta'(w_\zeta)w_\zeta^{(q+1)}\right|^2 dx + \frac{\alpha}{2}\|\zeta^{(s)}\|^2_{L^2([0,1])}$$

Unsurprisingly, this is the same minimization problem as (9), derived for spatially uniform discretizations of corresponding order. The reason is that space x and time t are interchangeable in a travelling wave solution, up to the constant wave speed factor.

4.2 Time Stepping

In this section we will briefly discuss the impact of pointwise nonlinear scaling on single step methods, in particular the extrapolated linearly implicit Euler scheme and Rosenbrock methods (cf. [6, 8]).

A difficulty introduced by the transition from (1) to (2) is the solution-dependent factor $\vartheta'(u_\zeta)$ in front of the time derivative $\partial_t u_\zeta$. Simplifying notation, in this section we will consider ODEs of the form

$$B(u)\partial_t u = f(u). \tag{13}$$

One step of the extrapolated linearly implicit Euler method on the time interval $[t_k, t_{k+1}]$ consists of integrating (13) from t_k to t_{k+1} on equidistant subgrids with step length $\tau_j = (t_{k+1} - t_k)/n_j$, resulting in values $u_{k+1}(\tau_j)$, and defining $u_{k+1} = u_{k+1}(0)$ by polynomial extrapolation. The linearly implicit Euler method on the subgrid j is defined as

$$(B(u_{k,j,i}) - \tau_j A_k)(u_{k,j,i+1} - u_{k,j,i}) = \tau_j f(u_{k,j,i}) \quad \text{for } i = 0, \ldots, n_j - 1 \tag{14}$$

with $u_{k,j,0} = u_k$ and $u_{k+1}(\tau_j) = u_{k,j,n_j}$. Here, A_k is an almost arbitrary approximation of $f'(u_k)$. Note that this method is a W-method, meaning that a deviation of A_k from $f'(u_k)$ does not affect the order of convergence of the extrapolated Euler, but only the error constant and the stability properties.

The solution of linear systems (14) with different matrices $B(u_{k,j,i}) - \tau_j A_k$ is required in every sub-timestep (j, i). The computational complexity can be reduced by iterative solution re-using a preconditioner or factorization of $B(u_{k,j,i}) - \tau_j A_k$

during the linearly implicit Euler method, see [7]. Still, the matrix $B(u_{k,j,i})$ needs to be computed, and the implementation is more complex than for constant B independent of u.

Rosenbrock methods are linearly and diagonally implicit Runge-Kutta methods. One step of an n-stage Rosenbrock method on the time interval $[t_k, t_{k+1}]$ of length $\tau_k = t_{k+1} - t_k$ is defined by

$$(B - \tau\beta_{jj}A_k)s_j = \tau_k A_k \sum_{i=1}^{j-1}(\beta_{ji} - \alpha_{ji})s_i + f\left(u_k + \tau_k \sum_{i=1}^{j-1}\alpha_{ji}s_j\right)$$

for $j = 1, \ldots, n$. These methods are attractive since they can be designed with $\beta_{jj} = \gamma$ for all j, such that only n linear systems with the same matrix $B - \tau_k\gamma A_k$ need to be solved. An important drawback is that Rosenbrock methods are not directly applicable to nonlinearly scaled systems (2) where B depends on u. However, one can rewrite (13) as a differential algebraic system

$$\begin{aligned} \partial_t u &= z \\ 0 &= f(u) - B(u)z, \end{aligned} \tag{15}$$

to which Rosenbrock methods can be applied directly (cf. [15]). Due to the special structure of (15), the auxiliary variable z can be eliminated analytically, which gives rise to a computationally cheap method.

The same is possible for the linearly implicit Euler method, which then reads

$$(B(u_k) - \tau_j A_k)(u_{k,j,i+1} - u_{k,j,i}) = \tau_j f(u_{k,j,i}) + (B(u_k) - B(u_{k,j,i}))(u_{k,j,i} - u_{k,j,i-1})$$

with $u_{k,j,-1} = u_{k,j,0}$. The advantage is that the linear equation systems to be solved feature the same matrix and only different right hand sides, and that only the application of the difference $B(u_k) - B(u_{k,j,i})$ to a vector needs to be computed. While this approach is computationally cheap and easy to implement, it has a significant drawback: Although the convergence order is retained, an increase in the error constant by a factor of 3 has been observed in the following examples. The reported results are therefore based on the direct approach (14) above.

A further important aspect is deliberate sparsing of the Jacobian. While the order of Rosenbrock methods in general relies on the exact value $A = f'(u_0)$, the extrapolated linearly implicit Euler method is a W-method and as such its order is independent of the approximation quality of $A \approx f'(u_0)$. Note that in general W-methods applied to PDEs are limited to second order [14], but can achieve higher orders for certain classes of problems. With the freedom of choosing A arbitrarily, we can modify the Jacobian in order to accelerate the linear solver on one hand, e.g. by dropping entries, or to reduce the error constant of the W-method on the other hand. Both aspects depend on the actual problem, and the optimal choice can thus depend on the chosen nonlinear transformation. Changes in the error constant by a factor of 10 have been observed in the numerical examples below.

		Euler ($q = 1$)			extrap. Euler ($q = 2$)		
t	k	$\|\varepsilon\|_{L_2}$	$\|\varepsilon_\zeta\|_{L_2}$	ratio	$\|\varepsilon\|_{L_2}$	$\|\varepsilon_\zeta\|_{L_2}$	ratio
15	1	9.55e-2	3.32e-3	26.6	7.66e-3	1.79e-3	4.3
	0	4.54e-2	2.32e-3	18.3	1.39e-3	4.85e-4	2.9
	-1	2.10e-2	1.30e-3	15.8	2.88e-4	1.27e-4	2.3
	-2	9.77e-3	6.61e-4	14.8	6.67e-5	3.27e-5	2.0
	-3	4.47e-3	3.15e-4	15.0	1.62e-5	8.20e-6	2.0
	-4	1.89e-3	1.36e-4	17.1	3.84e-6	1.97e-6	2.0
30	1	2.41e-1	9.05e-3	28.8	2.43e-2	4.34e-3	5.6
	0	1.42e-1	7.78e-3	19.6	5.15e-3	1.15e-3	4.5
	-1	7.08e-2	4.46e-3	16.1	1.13e-3	3.06e-4	3.7
	-2	3.38e-2	2.29e-3	14.8	2.60e-4	7.99e-5	3.3
	-3	1.64e-2	1.10e-3	14.2	5.89e-5	2.03e-5	2.9
	-4	8.15e-3	4.75e-4	13.9	1.06e-5	4.90e-6	2.2

Table 4: Time discretization error for uniform time steps $\tau = 2^k$ for the scalar reaction-diffusion equation (10).

The impact of nonlinear scaling on implicit multi-step methods, e.g. DASSL [17], is subject of future work.

4.3 Numerical Example

We revisit the example from Section 3.1.2, but now choose the discretizations such that the time integration error dominates. The final time is $T = 30$, the spatial discretization consists of quadratic finite elements on a uniform grid obtained by 6 levels of uniform refinement of $\bar{\Omega}$. For the time stepping we use the linearly implicit Euler scheme ($q = 1$) and its extrapolation to order $q = 2$ with step sizes $\tau = 2^k$, $k = -6, \dots, 1$. Deliberate sparsing has been examined with respect to dropping the diffusion or reaction terms of the Jacobian $\Delta + f'(u_0)$. The best choices turned out to be the full Jacobian for the original problem and to drop the reaction derivative for the scaled problem. The scalings ζ are the same as the one used in Section 3.1.2 for linear and quadratic finite elements, respectively, with predicted error reduction factors of 22 and 13. As before, the error has been approximated by the difference to the most accurate solution obtained ($k = -6$).

The estimated propagation errors at times 15 and 30 (see Fig. 3) are shown in Table 4. Clearly visible is a gain in accuracy. For the semi-implicit Euler method, the factor is below but in the order of magnitude as predicted for the ideal situation of a planar travelling wave. As before in the spatial discretization errors, the accuracy gain is somewhat smaller when the reaction fronts merge and the solution shape differs significantly from a travelling wave.

The picture is less clear for the second order scheme. Smaller gains are observed, and the deterioration with smaller time steps is more pronounced.

5 Scaling for Spatio-Temporal Discretization

Focusing on spatial or time discretization alone is bound to be suboptimal when we are interested in the accuracy of the integration of a reaction-diffusion equation involving simultaneous discretization in time and space. In the following we will combine the error and complexity models from sections 3 and 4 above into a joint optimization problem for designing nonlinear scalings.

We assume, quite pessimistically, that the spatial and temporal error densities add up, whereas the work is combined multiplicatively:

$$e_\zeta = e_{x\zeta} + e_{t\zeta} \quad \text{and} \quad W = W_x W_t$$

We focus on adaptive methods and therefore presume spatial error equilibration ($e_{x\zeta} \equiv c$) as well as equilibration of spatial discretization and propagation errors ($\|e_{x\zeta}\|_{L^2(\Omega)} = \|e_{t\zeta}\|_{L^2(\Omega)}$). Inserting (5) and (12) and dropping all constant factors that do not affect the minimizer, we end up with the optimization problem

$$\min_{\zeta \in Z} \left(\int_a^b \left| \vartheta'(w_\zeta) w_\zeta^{(p+1)} \right|^{\frac{d}{p+1}} dx \right) \left(\int_a^b \left(\vartheta'(w_\zeta) w_\zeta^{(p+1)} \right)^2 dx \right) + \frac{\alpha}{2} \|\zeta^{(s)}\|^2_{L^2([0,1])}$$

to be solved for the optimal scaling ζ.

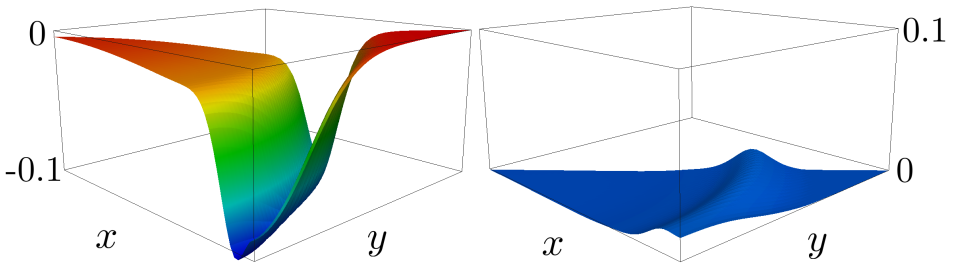

Figure 3: Time integration error of the unscaled (left) and scaled (right) solution for $\tau = 2$. Note that the error of the scaled solution is scaled back and hence directly comparable to the unscaled error.

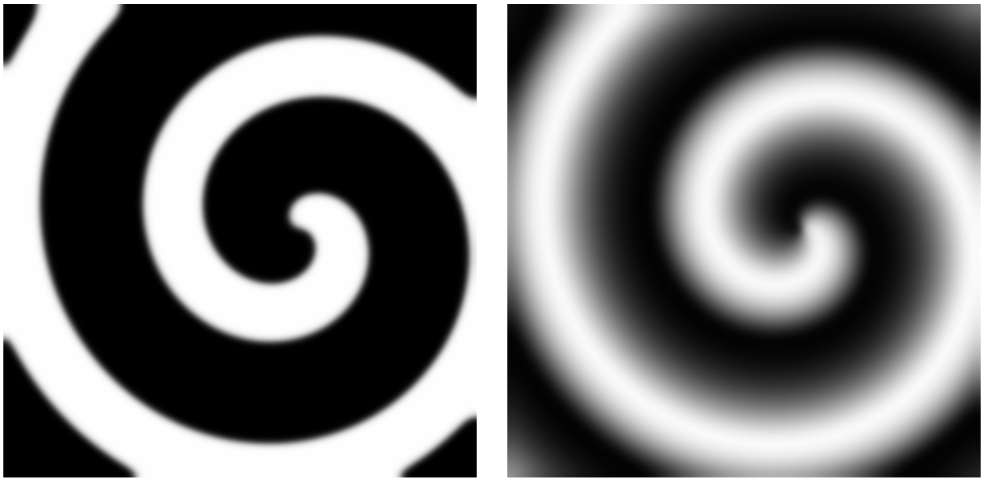

Figure 4: Spiral wave solution of (16) at $t = 20$. Left: u, right: v.

5.1 Numerical Example

Here we study the effect of nonlinear scaling of rotating spiral waves in an excitable medium. We employ the particularly simple Barkley model [3]

$$\begin{aligned} \partial_t u &= \kappa \Delta u + \epsilon^{-1} u(1-u)\left(u - \frac{v+b}{a}\right) \\ \partial_t v &= u - v \end{aligned} \tag{16}$$

on $\Omega = [-0.5, 0.5]^2$ with homogeneous Neumann boundary conditions. With $\epsilon = 0.01$, $\kappa = 0.002$, $a = 0.8$, $b = 0.01$, and the initial values $u_0(x) = \tanh(5r)\phi(\alpha)$, $v_0(x) = \tanh(5r)\phi(\alpha{+}.5)$ for $x = r(\cos\alpha, \sin\alpha)$, $r > 0$ with $\phi(\alpha) = \sum_{i\in\mathbb{Z}} e^{-2(\alpha+2i\pi)^2}$, the system develops a rotating spiral wave shown in Fig. 4. The small value of ϵ leads to a fast dynamic in u compared to v. The small value of κ subsequently results in small spatial scales in u. Thus, the dominant discretization error in both, time and space, originates from the u component. A mesh and time step that is sufficiently fine for u will be unnecessarily fine for discretizing v. Efficiency may be gained by using different meshes or time steps for u and v at the cost of a significantly more complex implementation (cf. [18]). Here we aim at a nonlinear scaling of u only that alleviates the discrepancy in required resolution, and thus permits an efficient discretization without the need for complex data structures.

The system (16) has a stable homoclinic left-travelling wave solution connecting the only stable fixed point $(0, 0)$ with itself (see Fig. 5 left). Since the leading upward and following downward fronts are fairly symmetric, we use the leading upward front for designing a suitable nonlinear scaling (Fig. 5 right), again with regularization parameter $\alpha = 10^{-8}$.

The problem has been solved for $t \in [0, 7]$ by Rothe's method, where first the time

is discretized according to a given time tolerance and the arising stationary elliptic problems are solved up to a given spatial tolerance using linear finite elements with adaptive mesh refinement. Both estimated errors are measured in the L^2-norm. In this example, the spatial tolerance is set to half of the time tolerance. The resulting time steps of the original and the scaled computation shown in Fig. 6 are comparable. For the stricter tolerance, the scaled problem leads to slightly smaller time steps, which can be attributed to the more complex nonlinearity arising in the scaled reaction-diffusion system. The number of grid points required to satisfy the spatial tolerance, however, are reduced by appropriate scaling by a factor of 3 to 5 as shown in Fig. 7.

6 Conclusion

Pointwise nonlinear scaling with optimized scalings adapted to planar travelling wave solutions can provide a significant error reduction for both, spatial and time discretization of reaction-diffusion equations. Factors of 4 to 20 are observed in numerical examples. Alternatively, the number of unknowns in spatial discretization and the number of time steps necessary for obtaining a given accuracy can be significantly reduced, factors of 3 to 10 are observed. Moreover, the nonlinear scaling technique barely interferes with the implementation of PDE solvers and hence can be easily combined with other techniques for improving efficiency, such as mesh adaptivity, multigrid solvers, higher order finite elements, or parallelization.

Drawbacks of the approach are the necessary preparatory work of computing travelling wave solutions, the limitation to reaction-diffusion solutions that are locally of similar shape to planar travelling waves in a large part of the domain, and the more complex structure of the equation to be solved, in particular with respect to time integration. But in cases where the technique is applicable and when computing time or memory requirement are the limiting factor, nonlinear scaling is very effective in improving computational efficiency.

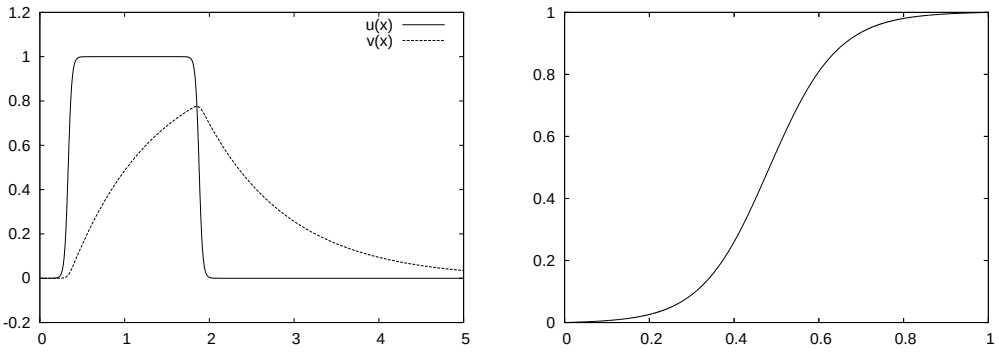

Figure 5: Travelling wave solution (left) and nonlinear scaling ζ^{-1} (right).

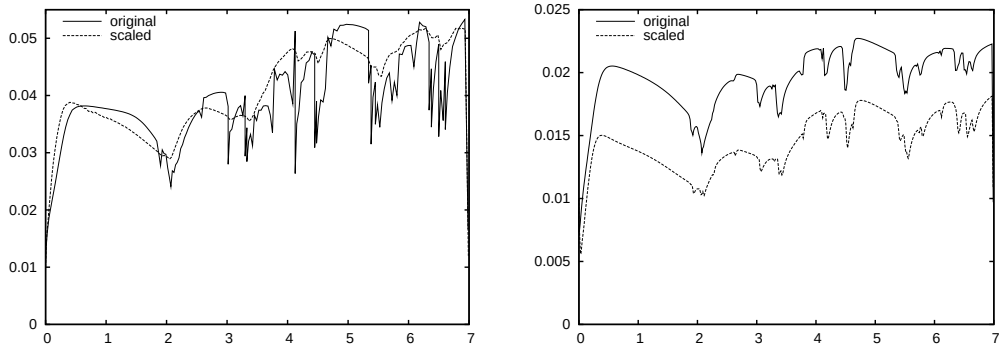

Figure 6: Time step sizes versus simulated time for the original and scaled equations for time tolerances 5e-3 (left) and 3e-4 (right).

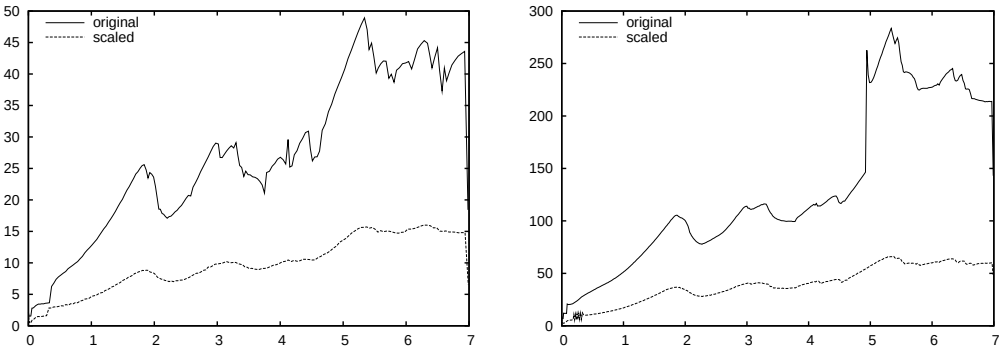

Figure 7: Grid vertices (in thousands) versus simulated time for the original and scaled equations for time tolerances 5e-3 (left) and 3e-4 (right).

Acknowledgement. The author would like to thank R. Roitzsch for computational assistance and J. Lang for helpful discussions and careful reading of the manuscript. This work has been supported by the DFG Research Center MATHEON "Mathematics for key technologies" in Berlin.

References

[1] T. Apel, S. Grosman, P. K. Jimack, and A. Meyer. A new methodology for anisotropic mesh refinement based upon error gradients. *Appl. Numer. Math.*, 50:329–341, 2004.

[2] M.J. Baines. *Moving Finite Elements.* Oxford University Press, Oxford, 1994.

[3] D. Barkley, M. Kness, and L.S. Tuckerman. Spiral-wave dynamics in a simple model of excitable media: The transition from simple to compound rotation. *Phys. Rev. A*, 42:2489–2492, 1990.

[4] P. Bastian, M. Blatt, A. Dedner, C. Engwer, R. Klöfkorn, M. Ohlberger, and O. Sander. A generic grid interface for parallel and adaptive scientific computing. Part I: Abstract framework. Technical report, 2007.

[5] P. Bastian, M. Blatt, A. Dedner, C. Engwer, R. Klöfkorn, M. Ohlberger, and O. Sander. A generic grid interface for parallel and adaptive scientific computing. Part II: Implementation and tests in DUNE. Technical report, 2007.

[6] P. Deuflhard and F.A. Bornemann. *Scientific Computing with Ordinary Differential Equations.* Texts in Applied Mathematics, vol. 42. Springer, New York, 2nd edition, 2002.

[7] P. Deuflhard and U. Nowak. Extrapolation integrators for quasilinear implicit ODEs. In P. Deuflhard and B. Engquist, editors, *Large Scale Scientific Computing*, pages 37–50. Birkhäuser, Boston, 1987.

[8] E. Hairer and G. Wanner. *Solving ordinary differential equations. II: Stiff and differential-algebraic problems. 2nd rev. ed.* Springer, Berlin, 1996.

[9] W. Hundsdorfer and J. Verwer. *Numerical solution of time-dependent advection-diffusion-reaction equations.*, volume 33 of *Series in Computational Mathematics.* Springer, Berlin, 2003.

[10] J.M. Hyman, S. Li, and L.R. Petzold. An adaptive moving mesh method with static rezoning for partial differential equations. *Comput. Math. Appl.*, 46(10-11):1511–1524, 2003.

[11] R. Kornhuber and R. Roitzsch. On adaptive grid refinement in the presence of internal and boundary layers. *IMPACT Comput. Sci. Engrg.*, 2:40–72, 1990.

[12] J. Lang. Adaptive FEM for reaction-diffusion equations. *Appl. Numer. Math.*, 26:105–116, 1998.

[13] J. Lang, W. Cao, W. Huang, and R.D. Russell. A two-dimensional moving finite element method with local refinement based on a posteriori error estimates. *Appl. Numer. Math.*, 46:75–94, 2003.

[14] Ch. Lubich and A. Ostermann. Linearly implicit time discretization of non-linear parabolic equations. *IMA J. Num. Anal.*, 15:555–583, 1995.

[15] Ch. Lubich and M. Roche. Rosenbrock methods for differential-algebraic systems with solution- dependent singular matrix multiplying the derivative. *Computing*, 43(4):325–342, 1990.

[16] U. Nowak. A fully adaptive MOL-treatment of parabolic 1-d problems with extrapolation techniques. *Appl. Numer. Math.*, 20:129–145, 1996.

[17] L.R. Petzold. A description of DASSL: A differential/algebraic system solver. In R.S. Stepleman, editor, *Scientific Computing*, pages 65–68. North-Holland, Amsterdam, 1983.

[18] A. Schmidt. A multi-mesh finite element method for phase field simulations. In H. Emmerich, B. Nestler, and M. Schreckenberg, editors, *Interface and Transport Dynamics - Computational Modelling*, volume 32 of *Lecture Notes in Computational Science and Engineering*, pages 208–217. Springer, Berlin, 2003.

[19] A. Wächter and L. Biegler. On the implementation of a primal-dual interior point filter line search algorithm for large-scale nonlinear programming. *Mathematical Programming*, 106(1):27–57, 2006.